8

Forming Free, Non-volatile and Reliable Bipolar Resistive Switching in Solution Processed Al/$BiFeO_3$/FTO

8.1 Introduction

BFO is a multiferroic material with ferroelectricity and anti-ferromagnetism existing together at room temperature (Spaldin et al., 2010). It has been synthesized by numerous methods such as PLD, sputtering, solution methods and spin coating for RRAM applications (Katiyar et al., 2015b)(You et al., 2014)(Bogle et al., 2016). It has shown both unipolar and bipolar switching behaviour with several switching mechanism explaining its RRAM behaviour (Katiyar et al., 2015b)(You et al., 2014)(Bogle et al., 2016). There is no consensus on type of switching and the type of switching mechanism as several explanations are available.

Spin coating is a simple cost effective technique which provides advantage of simple process and easy fabrication over other deposition technique. However depositing BFO using spin coating is a challenging process due to presence of secondary phases in the final annealed film (Zhang et al., 2016). Earlier, we have reported a spin coated BFO based RRAM with silver top electrode (TE) and FTO as bottom electrode (BE). This device showed robust RRAM characteristics with forming and the switching mechanism was assigned to formation and rupture of the filament formed due to silver ion migration. The device showed good reproducibility with low set and reset voltage together with reliability, as discussed in chapter 7 (Kumari et al., 2018b).

It is reported that the type of switching mechanism significantly depends on the work function difference between TE and BE as well because the interface at metal-insulator junction plays a crucial role in the switching phenomenon (Lin et al., 2011)(K.-J. Lee et al., 2015)(Young Jeong et al., 2011). This motivated us to understand the switching characteristics and mechanism of BFO RRAM with different metal top electrode. Previously, we have reported RRAM switching characteristics in Ag/BFO/FTO device configuration. The device showed bipolar RRAM characteristics and the switching mechanism was attributed to silver metal ion migration. Here, we investigated solution processed Al/BFO/FTO based RRAM device where aluminium is TE and FTO is BE. The device showed forming free, bipolar, non-volatile, RRAM characteristics. The devices showed excellent reliability and stability. The most interesting observation is the formation of AlOx interface layer between Al top contact and BFO layer in these RRAM devices.

8.2 Experiment

The film is synthesized by making a sol from bismuth nitrate pentahydrate ($Bi(NO_3)_3.5H_2O$, 98% Alfa Aser) and iron nitrate nonahydrate ($Fe(NO_3)_3.9H_2O$, 98% Alfa Aser) precursors in 2-Methoxyethanol (2-ME). 1.6 g of bismuth nitrate pentahydrate and 1.22 g of iron nitrate nonahydrate is dissolved into 10 ml of 2-ME. The solution is stirred for three hours at 80 °C. After that solution is aged overnight at room temperature. The FTO substrate is ultra-sonicated in acetone, isopropyl alcohol (IPA) and deionised (DI) water each for 15 minutes,

prior to deposition. The solution is spin coated on FTO glass at 3000 RPM for 30 seconds. After each deposition, the substrate is preheated at 350 °C for five minutes. The process is repeated 2 times to get the desired thickness of 70 nm. The schematic of deposition process is shown in figure 8.1. Finally, the deposited BFO film is heated at 450 °C for 3 hours in air.

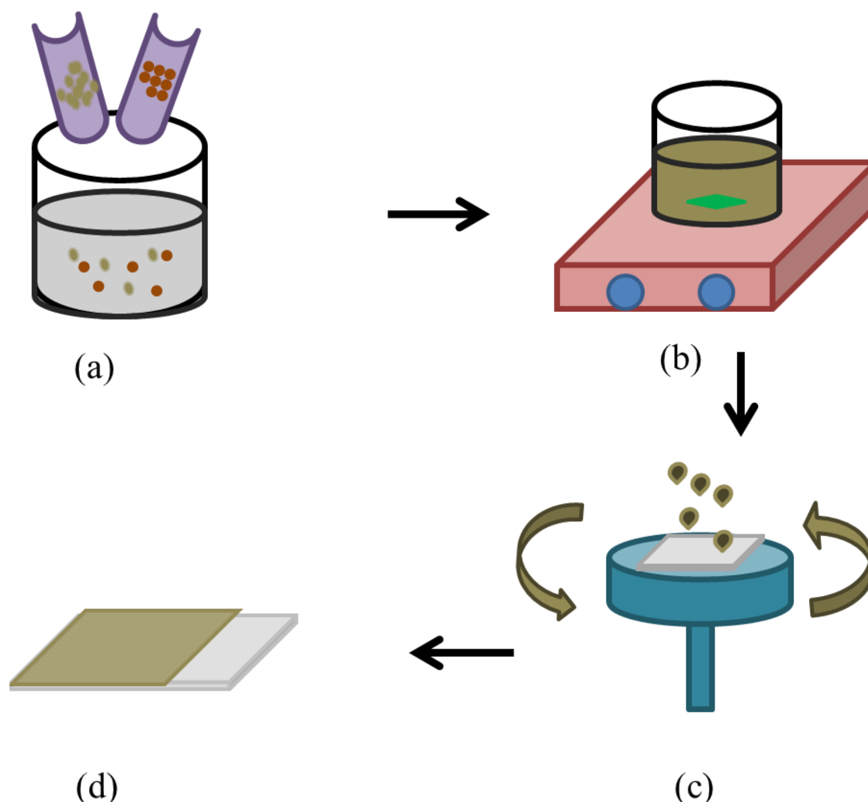

Figure 8.1: (a) Mixing of precursors in 2-ME, (b) Formation of BFO gel, (c) Spin coating of BFO gel on FTO glass and (d) BFO thin film after deposition

8.3 Results and Discussion

8.3.1 Structural and Microstructural Properties

The structural information of the film is analysed by Bruker powder XRD in 20-65° 2θ range The XRD pattern of BFO/FTO is shown in figure 8.2 (a). The XRD peaks are attributed to perovskite BFO (ICDD # 71-2494) without any secondary phase formation which indicates impurity free synthesis of BFO thin film. Other peaks belong to FTO substrate. The BFO thin film is indexed to rhombohedral phase. It shows a higher relative texturing along (104) plane.

The morphology of the BFO thin film is analysed by SEM which showed that the film is smooth and does not have any granular variations. The surface topology and roughness of the film are analysed using AFM. The calculated average and RMS roughness of the film is 9.5±2 nm and 9.16±1.5 nm, respectively, which substantiates the smoothness of the deposited film. Both these images are shown in figure 8.2 (b). The microstructural analysis substantiates good quality of the film for device applications.

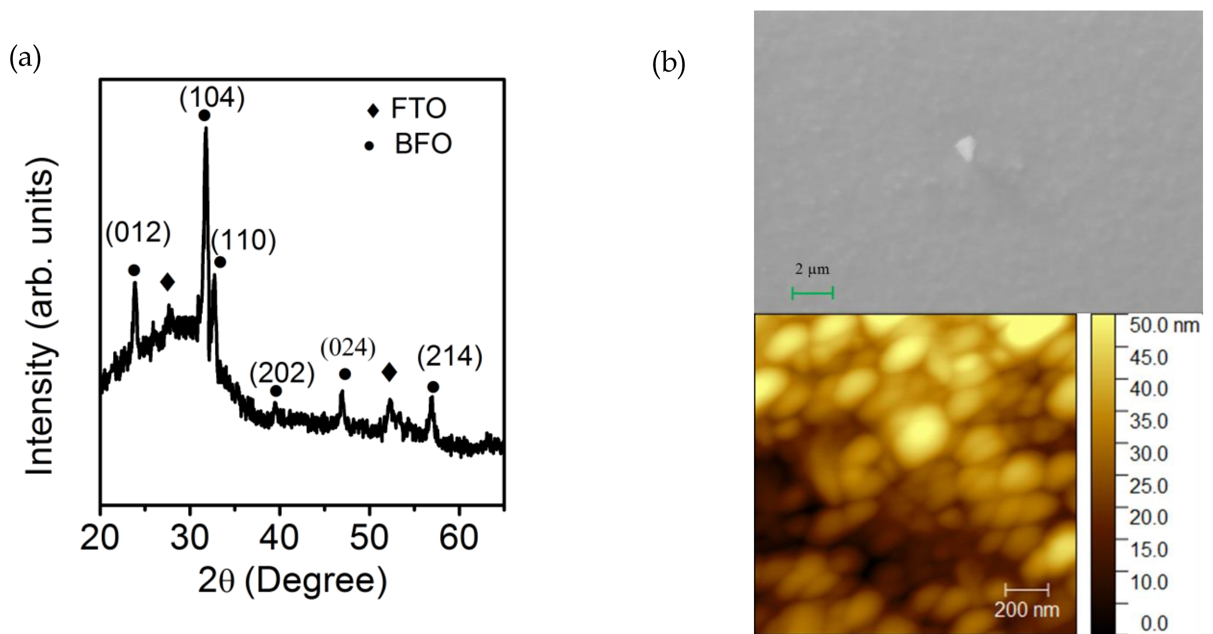

Figure 8.2: (a) XRD pattern of BFO and (b) SEM and AFM images of BFO

8.3.2 Optical Characterization

The absorption spectrum of BFO is obtained using Uv-Vis spectroscopy and it was further used to estimate the energy band gap of BFO by using Tauc plot. Tauc plot for a direct band gap is a curve between $(\alpha h\nu)^2$ and hv where, h is Plank's constant, α is absorption coefficient and v is frequency. The evaluated band gap is ~2.6 eV and the curve is shown in figure 8.3 (a). The calculated value of band gap matched well with the reported values (Sando et al., 2018b).

The structural and vibrational analysis of the BFO is done using Raman spectroscopy. At room temperature, BFO has rhombohedral structure consisting two formula units in a single rhombohedral primitive unit cell. It has 18 optical phonon modes, 13 of which are Raman active (Hashem and Hamed, 2018)(Gupta et al., 2014)(Muneeswaran et al., 2014). It is represented by the formula $\Gamma_{opt}=4A_1+5A_2+9E$, where A_2 modes are Raman inactive. Further, A_1 and E modes are classified into longitudinal (LO) and transverse (TO) modes. The A_1 modes in BFO are LO and E modes are TO. A_1(LO) and first and second order E(TO) modes represent contributions from Bi-O bonds. Third and fourth order E(TO) modes represent the contributions from Fe-O bonds. E(TO) substantiates the motion of atoms in "a" and "b" direction and A_1(LO) substantiated the motion of atoms along "c" axis (Gupta et al., 2014)(Muneeswaran et al., 2014). We observed 2 A_1 modes which are A_1-1 and A_1-2 corresponding to 137 and 168 cm^{-1} along with one E(TO) modes E_2 corresponding to 109 cm^{-1} (Gupta et al., 2014)(Muneeswaran et al., 2014) which is shown in figure 8.3 (b). These results match well with the reported literatures.

8.3.3 Electrical Characterization

The electrical characterizations of the devices are carried out using Keithley 4200 SCS. TE is subjected to positive voltage and BE is kept at ground potential. The applied bias is from -4 V→ 0 V→3 V→ 0 V→ -4 V on the Al/BFO/FTO device. The device configuration is shown in the inset of figure 5 (a). To shield the device from permanent breakdown, a compliance current (CC) of 20 mA is applied during the measurement. This device is forming free which is desirable as it requires low voltage leading to low power consumption. The device showed bipolar resistance switching with set voltage in negative side and reset voltage in positive side. The obtained resistive memory I-V curve is presented in figure 8.4 (a), indicating I_{on}/I_{off} ratio around one order of magnitude at -0.2 V. the device is swept in negative region from 0-(-4) V then the device current starts increasing. It is difficult to read accurate value of set voltage however a

substantial increase in current is visible around ~-1.3V and the device starts switching from low current to high current. This phenomenon brings HRS in to LRS and this is called set process.

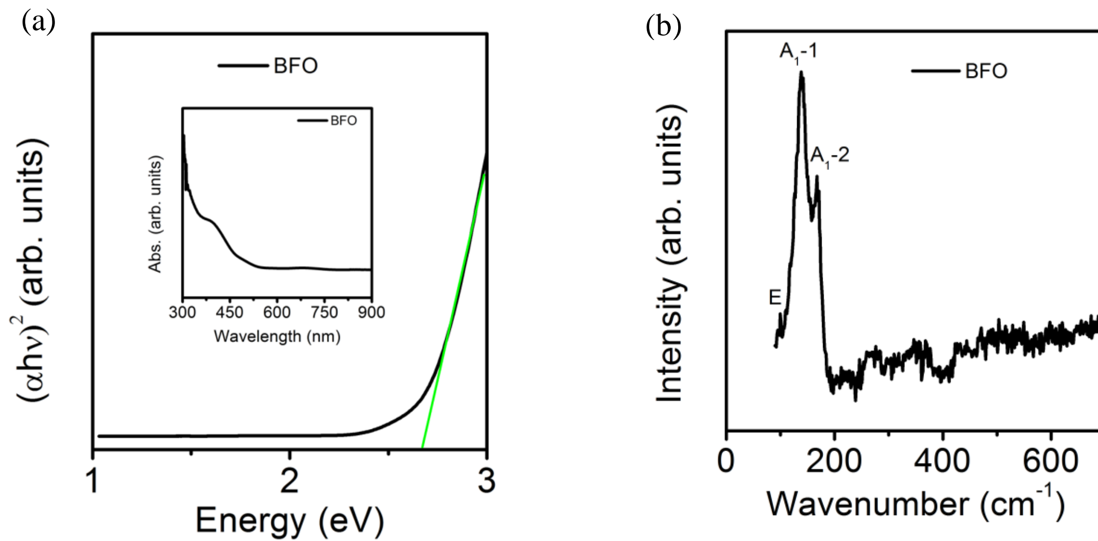

Figure 8.3: (a) Tauc plot of BFO with absorption spectra in inset and (b) Raman spectra of BFO

It is evident from the curve that set is not abrupt but it is gradual. The set voltage is V_{set}~-1.3V. When positive bias is applied, the current starts decreasing and at ~ 0.9 V, the resistance starts changing from LRS to HRS. This phenomenon is reset process and the observed reset voltage is V_{reset}=0.8 V, this process is also taking place gradually. This polarity dependent set and reset process substantiates bipolar resistive switching. This gradual set and reset which is taking place in our device is known as analog switching and has a great potential application in neuromorphic memory applications (T. Shi et al., 2016a). However, we did not do any detail study to see its potential to be used in such applications. The nonlinearity factor is defined as $I(V_{set})/I(1/2\ V_{set})$and is 5 for our device (Yuan et al., 2016)(Kim et al., 2017).

The devices showed reproducibility up to 256 cycles with slight variation in set and reset voltage. The graphs of multiple cycles are shown in figure 8.4 (b). This result substantiates that the devices are stable and can work without device failure. The retention curve of the devices is given in figure 8.4 (c). The graph depicts that how long the window of LRS and HRS is maintained without degradation and tells about the stability of the devices. The window was calculated for 10^4 seconds at 0.2 V in LRS and HRS states. We can see that the window is maintained in the entire time length without any degradation. This result substantiates the non-volatility of our devices.

The reliability of the device is analysed by using Weibull's distribution curve. The Weibulls's probability is given by the formula $\ln[-\ln\{1-F(V)\}]=\beta\ln(V)$ where, F(V) is set and reset voltage function and β is shape parameter(Kumari et al., 2018b) (Lawless, 1983). The graph is shown in figure 8.4 (d), suggesting the average value of V_{set} and V_{reset} are -1.31 V and 0.78 V, respectively. The smaller variation of V_{set} (0.23 V) and V_{reset} (0.14 V) substantiates that the devices are reliable. The calculated shape parameter β is ~19 and 34 for V_{set} and Vre_{set}, respectively. The higher value of β substantiates uniform distribution of set and reset voltages. Further, we plotted Weibull's distribution for LRS and HRS at 0.2 V, figure 8.5 (a). The LRS state demonstrates almost constant resistance for consecutive cycles however; a variation in HRS states is observed in the range of 3.5-6 kΩ. The average estimated value of LRS and HRS are ~480 Ω and ~4.7 kΩ, respectively.

The AC endurance of the devices are measured for 7100 AC pulses with pulse width 100 ms which is given in figure 8.5 (b). The alternate set and reset voltages of -3 V and 1 V was

applied to check device stability, respectively. It is clear from figure 8.5 (b) that the device was able to switch on and off alternatively with a smaller variation in ON and OFF currents.
The switching mechanism is understood by plotting the log (I)-log (V) graph for LRS and HRS which is shown in figure 8.5 (c). The HRS curve is divided into two regions. In the first region, the slope of the graph is 1 (I α V), supporting the ohmic conduction mechanism in the lower voltage side and in the higher voltage range I α $V^{2.5}$, supporting the trap assisted space charge limited (SCLC) conduction mechanism.

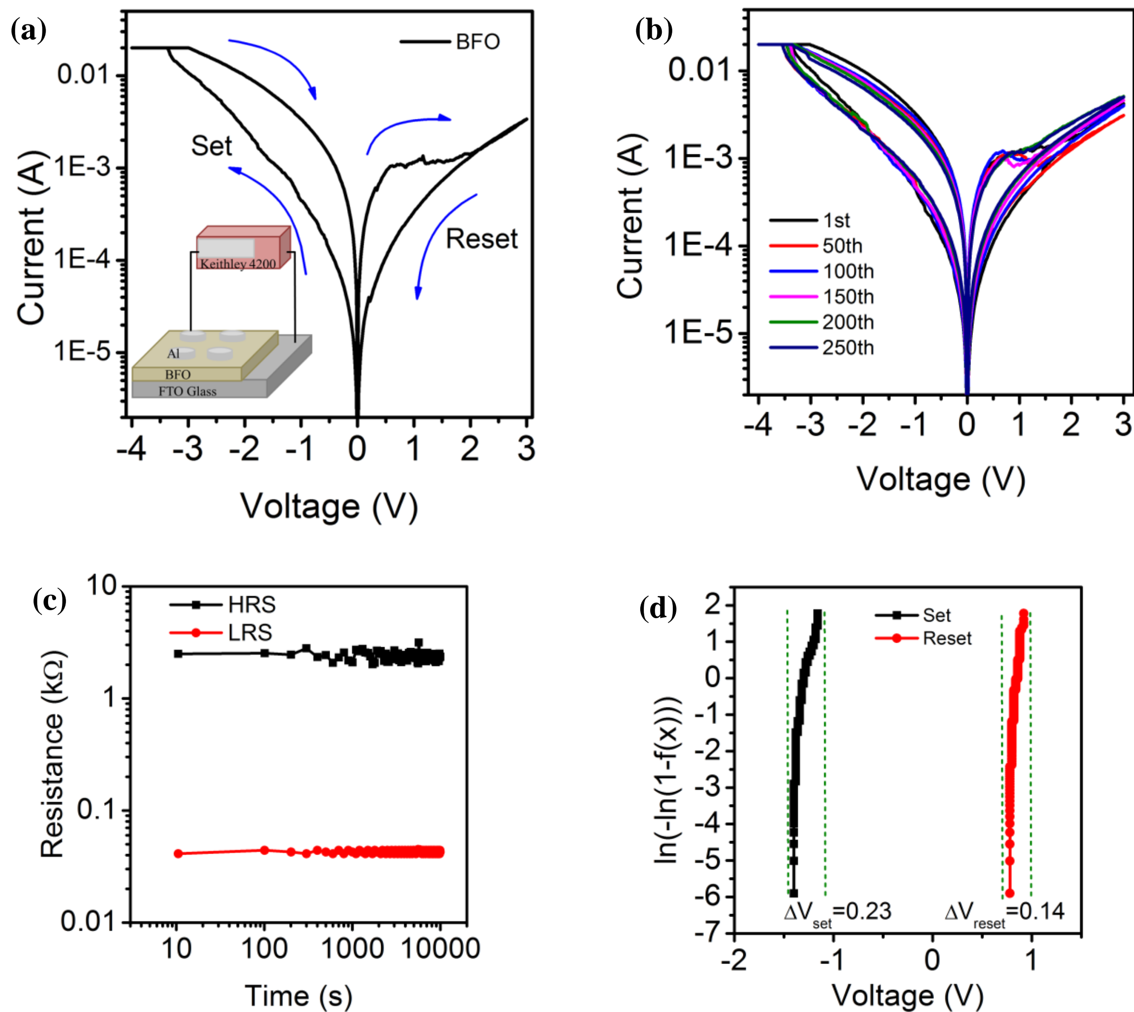

Figure 8.4: (a) Bipolar current-voltage characteristics , (b) Multiple cycles, (c) Retention curve and (d) Probability curve of BFO RRAM

The LRS side shows ohmic conduction mechanism. The different conduction mechanism for HRS and LRS substantiates that the switching is taking place due to filament formation (Kumari et al., 2018b). Similar type of conduction mechanism is observed for reset state which is shown in figure 8.5 (d). The filament formation can be from diffusion of metal ions or due to migration of oxygen vacancies and both are explained by SCLC conduction mechanism (Kumari et al., 2018b). BFO has intrinsic oxygen vacancies already present in the material. Presences of SCLC mechanism also indicate that interface plays an crucial role in carrier transport (Yuan et al., 2016). We have used aluminium as top contact and FTO as bottom contact which has work function 4.28 and 4.4 eV, respectively. The FTO BE behaves as oxygen vacancy reservoir which supplies and stores oxygen vacancies in resistive switching (T. Shi et al., 2016b). Aluminium is an easily oxidising material because of lower standard Gibbs free energy of formation (Young Jeong et al., 2011). Hence, aluminium reacts with oxygen present near the surface of BFO and

makes a thin layer of AlO_x near the interface of Al/BFO. This increases number of oxygen vacancies near the electrode/material interface (Chiang et al., 2012). This formation of AlO_x thin layer leads to forming free RRAM because of the enhanced oxygen vacancies. This interface contains large number of oxygen ions which is acquired from the BFO thin film leading to large slop. Based on these conclusions, the bipolar switching mechanism can be attributed to double reservoir model which has been reported earlier (Chiang et al., 2012).

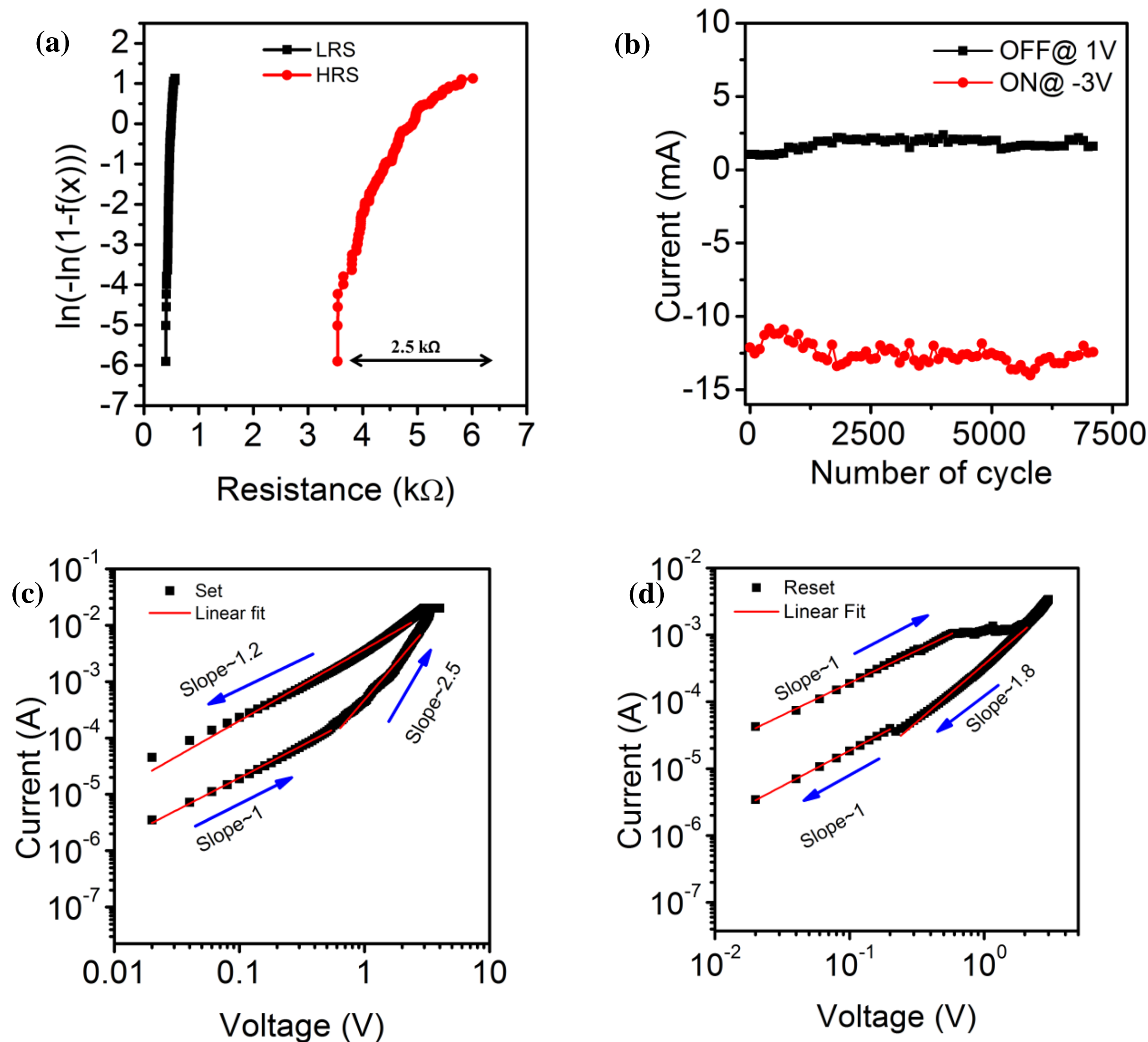

Figure 8.5: (a) Weibull's distribution curve of LRS and HRS @0.2 V (b) AC Endurance curve for 7000 cycles, (c) log I-log V curve of set state, (d) log I-log V curve of reset state

To understand the presence of AlO_x layer, we have done impedance spectroscopy on the Al/BFO/FTO in top and bottom configuration reset state. The applied frequency range is 1-10^5 Hz without any DC voltage bias. First we did the fitting without considering any interfacial layers and the measured Cole-Cole plot which is a graph between real and imaginary impedance is shown in figure 8.6 (a). The fitted equivalent circuit model is given in the inset of figure 8.6 (a). It is evident from the curve is that the fitting is not accurate which substantiates the presence of another layer. The fitting of the reset impedance spectroscopy with interfacial layer is shown in figure 8.6 (b). The fitted equivalent circuit for rest state is given in the inset of figure 8.6 (b). The lower side of frequency region is attributed to interface and higher side corresponds to thin film of BFO. It is evident from the circuit that a parallel combination of resistance (R_1=1.2 kΩ) and constant phase element (CPE, n=0.7) is present in series along with

parallel combination of capacitance (C_2=728 pF) and resistance (R_2=800 Ω) of BFO. This additional circuit is considered because of the presence of thin AlO_x layer at the interface of Al and BFO. AlO_x has high resistance in comparison to BFO because of high resistivity of BFO. The estimated resistivity value of AlOx is 4.7×10^4 Ω-m by considering the thickness of AlOx ~ 5nm. The estimated value is relatively lower than the actual reported value of pure alumina and the reason is attributed to defects present in AlO_x. Apart from that, resistivity of alumina is reported to decrease with increase in temperature which might be another reason for low estimated resistivity value as during set process, the temperature inside the film is elevated. Resistances R_0 and R_3 are contact resistances near Al/AlO_x interface and FTO/BFO interface and have a combined value of ~1.7 kΩ. The higher interface resistance near FTO/BFO interface leads to high voltage requirement for set process to realize the oxygen ion exchange at the interface. CPE is constant phase element which is a complex element and is a combination of resistance and capacitance and the value of capacitance is extracted from $C=(Q*R^{1-n})^{1/n}$, CPE is pure capacitor when n=1 and pure resistance when n=0. The CPE has value of n=0.7 and is present because of the bilayer and when distributed elements are present inside the AlO_x layer (Cesiulis et al., 2016).

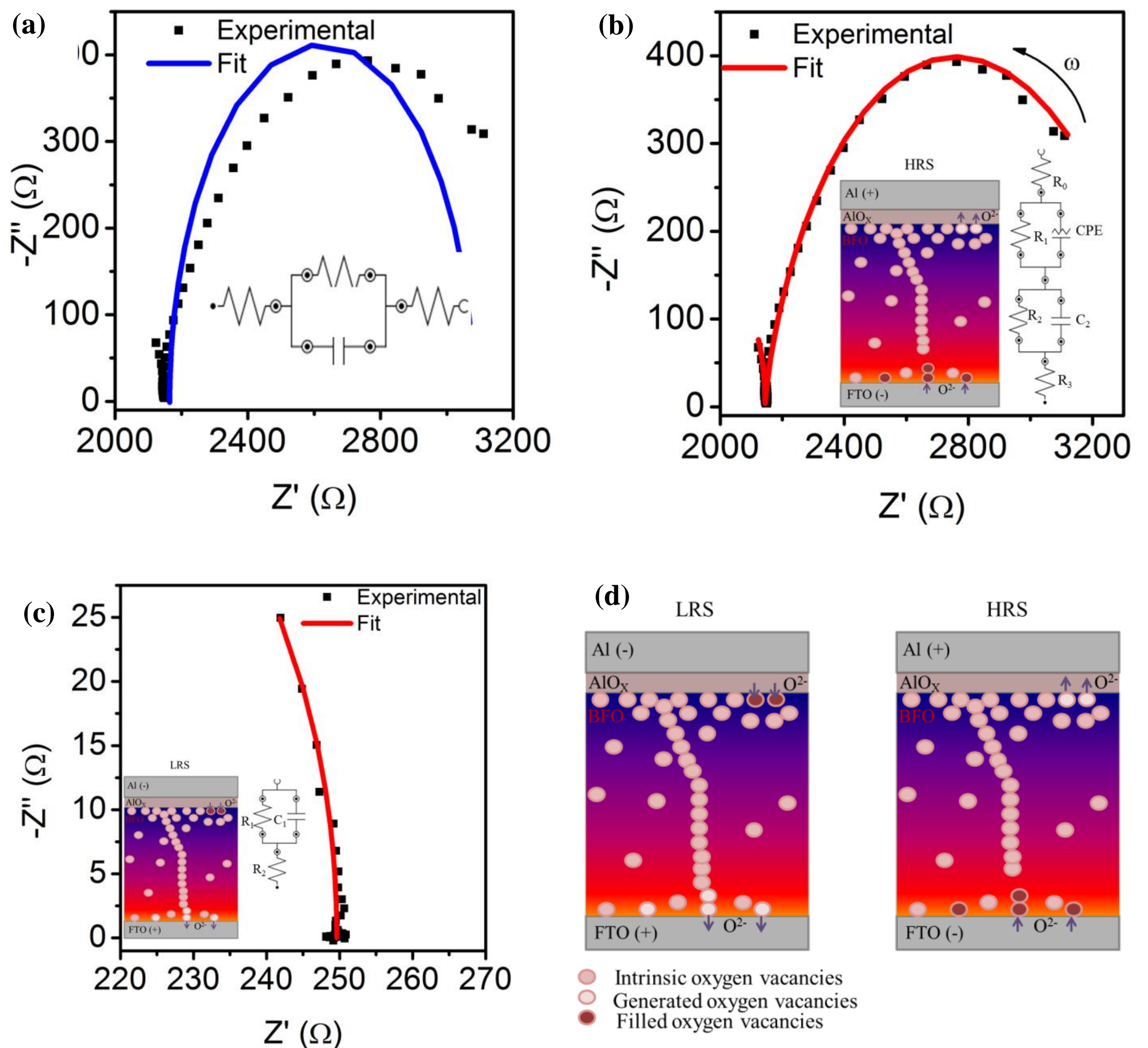

Figure 8.6: (a) Impedance curve fitting of HRS without R_1 and CPE, (b) Impedance cure fitting of HRS with R_1 and CPE, (c) Impedance curve fitting of LRS and (d) Schematic of filament formation mechanism

The impedance curve of set process is shown in the figure 8.6 (c) and shows a slightly tilted straight line with most of the points accumulated at the bottom of the line. The equivalent circuit of set process is given in the inset of figure 8.6 (c). This graph confirms the filament formation inside the device. It has a parallel combination of resistance (R_1=870 Ω) and capacitance (C_1=575 pF) which is coming due to the presence of AlO_x layer. We can see that the CPE in the AlO_x layer, which was present during reset state, is now replaced by pure capacitor in set state. This capacitor is present because the filament is being formed from the FTO/BFO interface to AlO_x-BFO interface and is not penetrating through the entire AlO_x surface. The resistance value of AlO_x layer is decreased in set state in comparison to reset state because of the oxygen ion migration in AlO_x during set process. The series resistance (R_0=1.63 Ω) is the combination of filament resistance as well as contact resistances. The capacitance of BFO is replaced by a resistance because of the filament formation. The BFO resistance is ~250 Ω in set which is very small to the value of BFO resistance in reset confirming the filament formation.

The schematic of the switching mechanism is presented in figure 8.6 (d). Here, by applying negative bias at aluminium electrode, O^{2-} migrates from the AlO_x-BFO interface towards the BFO and fills some oxygen vacancies. Also, since number of vacancies are large near the AlO_x-BFO interface, all the vacancies will not be filled and accumulation of oxygen vacancies will become a part of electrode (Chiang et al., 2012)(Kumar et al., 2017). Also the negative bias will push the oxygen ions toward FTO. When oxygen ions will move in FTO, it will leave oxygen vacancies near the BFO-FTO interface. These generated oxygen vacancies will align from FTO toward BFO-AlO_x interface and combine with the oxygen vacancies present near AlO_x. This will facilitate oxygen vacancies filament formation, resulting in a conducting path and device will be switching from HRS to LRS. This will bring the device in set state. The set voltage is higher because it needs relatively higher voltage to push the oxygen ions into FTO (Chiang et al., 2012)(Kumar et al., 2017). Further, by applying positive potential at the TE, oxygen ions will be pushed into AlO_x. This will generate the oxygen vacancies near AlO_x region. It will also push oxygen ions from FTO towards aluminium. Few oxygen ions will fill the vacancies of the conducting path near FTO and hence, will lead to rupture of oxygen vacancy filament. This will bring the device in reset state. The reset voltage is low because the oxygen ions near the FTO and thus, need smaller energy to fill the vacancies near FTO-BFO interface(Chiang et al., 2012).

8.4 Conclusion

In summary, we showed solution processed Al/BFO/FTO based RRAM devices with excellent reproducibility and reliability for 256 cycles or more. The results substantiate one order I_{on}/I_{off} ratio and the set and reset voltages are ~-1.3 V and 0.8 V, respectively. The non-volatile nature of the device is confirmed by measuring retention for 10^4 seconds. The endurance test for 7100 cycles substantiates the stability of the devices. The conduction mechanism is attributed to SCLC and ohmic conduction substantiating the formation and rupture of filament. Impedance analysis suggested that an AlOx layer is present at Al/BFO interface. The switching mechanism is attributed to oxygen filament formation assisted by AlOx layer present at the metal-insulator interface.